

KEK-TH-490  
 KEK Preprint 96-87  
 MPI-PhT/96-79  
 hep-ph/9607466  
 Revised Version

# One Loop Supersymmetric QCD Radiative Corrections to the top quark production in $p\bar{p}$ collisions

S.Alam<sup>1</sup>, K. Hagiwara<sup>1,2</sup>, and S. Matsumoto<sup>1</sup>

<sup>1</sup>*Theory Group, KEK, Tsukuba, Ibaraki 305, Japan*

<sup>2</sup>*Max-Planck-Institut für Physik,  
 Föhringer Ring 6, 80805 München, Germany*

## Abstract

The purpose of this note is to give the one loop radiative corrections to the top quark pair production in the  $p\bar{p}$  annihilation at the Fermilab Tevatron in the context of the Minimal Supersymmetric Model. We concentrate here on the supersymmetric QCD corrections and give the analytic expression for these corrections. Recently Li et. al. have reported the supersymmetric QCD corrections to this process we indicate clearly a comparison of their and our work. In particular, we find additional corrections [crossed box and gluon self-energy] at the one loop level which are not given by Li et. al.. Our numerical results disagree with the original claim of Li et. al. The numerical values given by them in a recent erratum do agree with the general trend of our numerical results however the actual values still disagree. We find that the percentage corrections at the hadronic corrections changes from 22% to  $-0.5\%$  as the squark mass is changed from 100 GeV to 600 GeV, for a gluino mass of 200 GeV. For a gluino mass of 150 GeV the squark-mass dependence is less abrupt; they change from  $-5.3\%$  to 1% as the squark mass is varied between 100 GeV and 600 GeV. We also present numerical results for differential cross section at the hadronic level, and percentage corrections at the parton level.

14.65.Ha, 12.38.Bx, 12.60.Jv, 13.85.-t

Typeset using REVTeX

## I. INTRODUCTION

As is well known by now the top quark existence has been experimentally shown by the CDF [1] and D0 [2] at almost 100% confidence level. Two interesting parameters, the mass of top and the cross section for top pair production, have been found as follows: by the CDF [1]

1.  $m_t^{\text{expt.}} = 176 \pm 9 \text{ GeV},$
2.  $\sigma_{t\bar{t}}^{\text{expt.}} = 7.6_{-1.5}^{+1.9} \text{ pb}.$

The D0 [2] finds for the same parameters

1.  $m_t^{\text{expt.}} = 170 \pm 18 \text{ GeV},$
2.  $\sigma_{t\bar{t}}^{\text{expt.}} = 5.2 \pm 1.8 \text{ pb}.$

The standard model theoretical predictions for the top pair production cross section is, assuming a top mass of 170 and 175 GeV [3],

1.  $\sigma_{t\bar{t}}^{\text{theory}} = 6.48_{-0.48}^{+0.09} \text{ pb}, m_t = 170 \text{ GeV},$
2.  $\sigma_{t\bar{t}}^{\text{theory}} = 5.52_{-0.42}^{+0.07} \text{ pb}, m_t = 175 \text{ GeV}.$

A theoretical fit based on the Standard Model Electroweak Precision calculations gives for the top mass the following limits [4]

$$m_t = 179 \pm 7_{-22(m_H=60 \text{ GeV})}^{+19(m_H=1000 \text{ GeV})} \mp 2(\alpha_s) \mp 5(\delta_\alpha) \quad (1)$$

here  $\alpha_s = 0.120 \pm 0.07$  and  $\delta_\alpha = 0.03 \pm 0.09$  are the uncertainties in  $\alpha_s(m_Z)$  [5] and  $\alpha(m_Z^2)$  [6], respectively.

Once the main injector upgrade becomes operational in 1999 [7] at Fermilab, the experimental sensitivity will be highly increased. For example the uncertainty in the production cross section will be reduced to 6-11%. The top mass uncertainty will be reduced to around 1-2%. Clearly the agreement between standard model theory and experimental results is not close enough to include moderate shifts from the SM results.

We have considered the complete one loop SUSY corrections to the process  $q\bar{q} \rightarrow t\bar{t}$ . These include SUSY-QCD and SUSY-QFD corrections not ignoring the box [both direct and crossed boxes]. Although box diagrams in general give a small contributions one must include them for completeness and exact numerical predictions. The purpose of this note is to concentrate on the complete one loop supersymmetric QCD corrections. Recently Li et. al. [8] have reported the one loop SUSY-QCD corrections. We give a comparison between their and our work. In particular we find additional corrections [crossed box and gluon self-energy] which are not given by them. Several mistakes/misprints in their work are also noted, however their erratum [8] now corrects these. Importantly our numerical work does not agree with their original claim [8]. However their numerical values given in the erratum [8] agrees now with the general trend that we give in this report. There still remains some disagreements as we report in section 4. We also give the energy dependence of the cross section and differential cross sections at the parton level. This allows us to compare our results with the one loop correction to the same subprocess in the standard model [9]. One may use the parton level values to study the details of the SUSY corrections more directly.

The one loop Electroweak corrections to the process  $q\bar{q} \rightarrow t\bar{t}$  have been considered by several groups [10] in the context of MSSM. Our results on these will be presented in a subsequent paper. The complete SUSY corrections to the processes  $q\bar{q} \rightarrow q\bar{q}$ ,  $q\bar{q} \rightarrow q\bar{q}$ ,  $q\bar{q} \rightarrow g\bar{g}$ , and  $q\bar{q} \rightarrow q\bar{q}$  are being considered by [11].

The layout of this paper is as follows. In next section we give the one loop SQCD

radiative corrections to the process  $q\bar{q} \rightarrow t\bar{t}$  which arise from the gluon self-energy, the quark wave function renormalization and the triangle diagrams. For completeness we also include the Born expression for the process  $q\bar{q} \rightarrow t\bar{t}$ . In Sec. 3, we write out the results for the corrections arising from the box diagrams [direct and crossed] due to the squarks and gluinos. Sec. 4 gives the numerical results. For our numerical work we use the Fortran code FF [12] for the evaluation of the scalar integrals [13], and the MRSA parton distributions of Martin et. al. [14] and finally the integrations are carried out by using BASES [15]. We have made several cross checks to make sure to eliminate any numerical errors. In the appendix we give the box contribution using the same momentum assignment of [8]. We compare our results with [8] wherever required.

## II. TREE, AND THE ONE-LOOP CONTRIBUTIONS IN SQCD [EXCEPT FOR BOX ] TO THE PROCESS $q\bar{q} \rightarrow t\bar{t}$ .

At the parton level the processes responsible for the production of top[t] anti-top[ $\bar{t}$ ] in energetic  $p\bar{p}$  collisions to order  $[\alpha_s^2]$  i.e. tree-level] are

- The annihilation of quark-antiquark pair into top anti-top via a virtual gluon exchange

$$q[p_1]\bar{q}[p_2] \rightarrow t[p_3]\bar{t}[p_4]$$

- The fusion of gluon-pair into top anti-top via a virtual gluon or a virtual top-quark exchange

$$g[p_1]g[p_2] \rightarrow t[p_3]\bar{t}[p_4]$$

Particle momenta have been shown in the parentheses. The schematic diagram for the first process is shown in Fig. 1, which is the reaction we choose to concentrate in this paper. To get a complete analysis one must include the second process as is done for the standard model [9], although it contributes only 10% at the Tevatron. We work with the Mandelstam variables  $s$ ,  $t$ , and  $u$  defined as

$$\hat{s} = (p_1 + p_2)^2 = (p_3 + p_4)^2, \quad (2)$$

$$\hat{t} = (p_1 - p_3)^2 = (p_4 - p_2)^2, \quad (3)$$

$$\hat{u} = (p_2 - p_3)^2 = (p_4 - p_1)^2 \quad (4)$$

The Mandelstam variables satisfy the relation  $\hat{s} + \hat{t} + \hat{u} = 2m_t^2$  where we have taken the initial parton mass as zero. With our momentum assignments the leading order QCD matrix element of quark antiquark annihilation is given by

$$iM_{\text{Born}}^{q\bar{q}} = \bar{u}_t^j(p_3, s_3)[-ig_s T_{ji}^c \gamma_\mu] v_t^l(p_4, s_4)[-i\frac{g^{\mu\nu}}{\hat{s}}] \bar{v}_q^k(p_2, s_2)[-ig_s T_{ki}^c \gamma_\nu] u_q^i(p_1, s_1) \quad (5)$$

It is straightforward to obtain from the above equation the square of the Born matrix element averaged over initial spin and color degrees of freedom and summed over the final ones. We immediately obtain

$$\sum |M_{\text{Born}}^{q\bar{q}}|^2 = |M_0|^2 = \frac{4g_s^4}{9\hat{s}^2} F_1 \quad (6)$$

here and elsewhere in this paper we define

$$F_1 = 2\hat{s}m_t^2 + (\hat{t} - m_t^2)^2 + (\hat{u} - m_t^2)^2 \quad (7)$$

The Born differential cross section is readily written as

$$\frac{d\sigma_0^{\text{Born}}}{d\hat{t}} = \frac{1}{16\pi\hat{s}^2} |M_0|^2 \quad (8)$$

Using the above equation to integrate over  $\hat{t}$ , and noting that the integration limits of  $\hat{t}$  are in our case are given by the equation

$$m_t^2 - \frac{1}{2}\hat{s} - \frac{1}{2}\hat{s}\beta_t \leq \hat{t} \leq m_t^2 - \frac{1}{2}\hat{s} + \frac{1}{2}\hat{s}\beta_t \quad (9)$$

[here  $\beta_t = \sqrt{1 - \frac{4m_t^2}{\hat{s}}}$ ] one immediately has for the expression for the Born cross section at the parton level

$$\sigma_0^{\text{Born}} = \frac{4\pi\alpha_s^2}{3\hat{s}^2} \left[\frac{2}{9}\right] \beta_t [\hat{s} + 2m_t^2] \quad (10)$$

We have intentionally written the above result in the form with the color factor separated out. The total amplitude squared upto one loop can be written as

$$|M_{0+1}|^2 = |M_0|^2 + 2\text{Re}[M_{\text{sew}}M_0^\dagger + M_{\text{triangle}}M_0^\dagger + M_{\text{box}}M_0^\dagger] \quad (11)$$

The total self-energy and wave-function renormalization [sew] contribution to the process  $q\bar{q} \rightarrow t\bar{t}$  can be written as

$$M_{\text{sew}}M_0^\dagger = M_{\text{SQCD}}^{\text{gluon}}M_0^\dagger + M_{\text{SQCD}}^{\text{w}}M_0^\dagger \quad (12)$$

The gluon self energy diagram is shown in Fig. 2a. We renormalize the SUSY contribution to the QCD coupling  $\alpha_s$  at zero momentum transfer. The gluon self-energy gets contribution from a gluino loop and s-quark loop. One may write

$$M_{\text{SQCD}}^{\text{gluon}}M_0^\dagger = M_{\tilde{g}}^{\text{gg}}M_0^\dagger + M_{\tilde{q}}^{\text{gg}}M_0^\dagger \quad (13)$$

$$M_{\tilde{g}}^{\text{gg}}M_0^\dagger = |M_0|^2 \frac{\alpha_s}{\pi} (3) \int_0^1 x(1-x) \ln[1 - x(1-x) \frac{\hat{s}}{m_{\tilde{g}}^2}] \quad (14)$$

$$M_{\tilde{q}}^{\text{gg}}M_0^\dagger = |M_0|^2 \frac{\alpha_s}{4\pi} \left(\frac{1}{2}\right) \int_0^1 \sum_{\text{flavor}} (1-2x)^2 \ln[1 - x(1-x) \frac{\hat{s}}{m_{\tilde{q}_1}^2}] \quad (15)$$

The sum over two complex scalar fermions [16],  $\tilde{f}_1$  and  $\tilde{f}_2$ , for each flavor is understood. For light quarks, the mass eigenstates are expected not to deviate significantly from the current eigenstates,  $\tilde{f}_L$  and  $\tilde{f}_R$ , due to chiral invariance. This may not be the case for the bottom and top squarks. To avoid plethora of indices we write all our results for the s-particle 1. However one must be careful that the total results do not always follow by replacing 1 by 2, for example in the box diagram we can have the mixed case i.e we may have squark [mass eigenstate 1] on one side and stop [mass eigenstate 2] on the other side of the box. We denote the squark mixing angle by  $\tilde{\theta}$  and that of stop by  $\theta$ . The expressions for squark and stop mass eigenstates are

$$\tilde{q}_1 = \tilde{q}_L \cos \tilde{\theta} + \tilde{q}_R \sin \tilde{\theta} \quad (16)$$

$$\tilde{q}_2 = -\tilde{q}_L \sin \tilde{\theta} + \tilde{q}_R \cos \tilde{\theta} \quad (17)$$

$$\tilde{t}_1 = \tilde{t}_L \cos \theta + \tilde{t}_R \sin \theta \quad (18)$$

$$\tilde{t}_2 = -\tilde{t}_L \sin \theta + \tilde{t}_R \cos \theta \quad (19)$$

The wavefunction renormalization [Fig. 2 a-d] contribution can be written as sum of two terms

$$M_{\text{SQCD}}^w M_0^\dagger = M^{\text{wt}} M_0^\dagger + M^{\text{wq}} M_0^\dagger \quad (20)$$

the [wt] contribution comes from the top wave-function renormalization and [wq] is from the parton [quark] wave function.

$$M^{\text{wt}} M_0^\dagger = |M_0|^2 \frac{\alpha_s}{3\pi} [A_t^2 (B_1(m_t^2, m_{\tilde{g}}, m_{\tilde{t}}) + 2m_t^2 B_1') - B_t^2 (2m_{\tilde{g}} m_t B_0')] \quad (21)$$

$$A_t^2 = a_1^2 + b_1^2 \quad (22)$$

$$B_t^2 = a_1^2 - b_1^2 \quad (23)$$

$$a_1 = \frac{1}{\sqrt{2}}(\cos \theta - \sin \theta)$$

$$b_1 = \frac{1}{\sqrt{2}}(\cos \theta + \sin \theta)$$

$$M^{\text{wq}} M_0^\dagger = |M_0|^2 \frac{\alpha_s}{3\pi} [A_q^2(B_1(0, m_{\tilde{g}}, m_{\tilde{q}}))] \quad (24)$$

$$A_q^2 = \tilde{a}_1^2 + \tilde{b}_1^2 \quad (25)$$

and  $B_q$  to be used below is given by

$$B_q^2 = \tilde{a}_1^2 - \tilde{b}_1^2 \quad (26)$$

$$\tilde{a}_1 = \frac{1}{\sqrt{2}}(\cos \tilde{\theta} - \sin \tilde{\theta})$$

$$\tilde{b}_1 = \frac{1}{\sqrt{2}}(\cos \tilde{\theta} + \sin \tilde{\theta})$$

The total Triangle contribution to the process  $q\bar{q} \longrightarrow t\bar{t}$  can be written as

$$M_{\text{triangle}} M_0^\dagger = M_{T1} M_0^\dagger + M_{T2} M_0^\dagger + M_{T3} M_0^\dagger + M_{T4} M_0^\dagger \quad (27)$$

where [Fig. 3a]

$$M_{T1} M_0^\dagger = \frac{4g_s^4}{9\hat{s}^2} \sum_i F_i^{T1} \quad (28)$$

Here  $i=1,2$

$$F_1^{T1} = \frac{\alpha_s}{24\pi} [2m_{\tilde{g}} m_t (B_t^2) [C_0 + C_{11}] - 2m_t^2 (A_t^2) [C_{21} + C_{11}] - 2(A_t^2) C_{24}] F_1 \quad (29)$$



$$F_2^{T1} = \frac{\alpha_s}{24\pi} [-2m_{\tilde{g}}m_t(B_t^2)[C_0 + C_{11}] + 2m_t^2(A_t^2)[C_{21} + C_{11}]]F_2$$

$$F_2 = \hat{s}^2 \quad (30)$$

We note that Li et. al. [8] have written  $2\hat{s}m_t^2 + \hat{s}^2 + \hat{s}(\hat{s} - 2m_t^2)$  as the coefficient of their  $F_5$  which is equal to  $2\hat{s}^2$ . In the above Eqs.29 and 30 the arguments of the C integral are  $C_{ij}(-p_3, p_5, m_{\tilde{g}}, m_{\tilde{t}_1}, m_{\tilde{t}_1})$ .

The expression for  $M_{T2}M_0^\dagger$  [Fig. 3b] is rather simple. We can simply obtain it from the above by setting  $m_t = 0$ . As a double check we have also calculated it directly and the result reads

$$M_{T2}M_0^\dagger = \frac{4g_s^4}{9\hat{s}^2} \sum_i F_i^{T2} \quad (31)$$

Here only  $i=1$  case is nonzero

$$F_1^{T2} = \frac{\alpha_s}{24\pi} [-2(A_q^2)C_{24}]F_1 \quad (32)$$

In the above Eq.32 the arguments of the C integral are  $C_{ij}(-p_1, p_5, m_{\tilde{g}}, m_{\tilde{q}_1}, m_{\tilde{q}_1})$ .

We now give the expression for Fig. 3c

$$M_{T3}M_0^\dagger = \frac{4g_s^4}{9\hat{s}^2} \sum_i F_i^{T3} \quad (33)$$

Here  $i=1,2$

$$F_1^{T3} = \frac{\alpha_s}{24\pi} [9] [-2m_{\tilde{g}}m_t(B_t^2)[C_0 + C_{11}] + (A_t^2)[[n-2]C_{24} - \hat{s}(C_{23} - C_{22})$$

$$- m_t^2(C_0 + C_{21} + 2C_{11}) - m_{\tilde{g}}^2 C_0]]F_1 \quad (34)$$

$$F_2^{T3} = \frac{\alpha_s}{24\pi} [9] [2m_{\tilde{g}}m_t(B_t^2)C_{11} + 2(A_t^2)[m_t^2(C_{11} + C_{21})]]F_2 \quad (35)$$

In the above Eqs.34 and 35 the argument of the C integral are  $C_{ij}(-p_3, p_5, m_{\tilde{t}_1}, m_{\tilde{g}}, m_{\tilde{g}})$ .

The triangle diagram for the  $qqg$  vertex is calculated directly and also as double check got from T3, by first replacing  $m_t$  by  $m_q$  and then setting the latter equal to zero. One obtains

$$M_{T4}M_0^\dagger = \frac{4g_s^4}{9\hat{s}^2} \sum_i F_i^{T4} \quad (36)$$

Here  $i=1$

$$F_1^{T4} = \frac{\alpha_s}{24\pi} [9][(A_q^2)[[n-2]C_{24} - \hat{s}(C_{23} - C_{22}) - m_{\tilde{g}}^2 C_0]] F_1 \quad (37)$$

In the above, Eq.37, the arguments of the C integral are  $C_{ij}(-p_1, p_5, m_{\tilde{q}_1}, m_{\tilde{g}}, m_{\tilde{g}})$ .

One can see from the above contributions of self energy ,wave function renormalization and triangles that they all factor into something times tree level amplitude except for contributions from triangle diagrams, Eqs.30 and 35. These arise since the top mass cannot be ignored! From the arguments of the above loop integrals we see immediately that they do not depend on the t-channel variable. From these simple observations one can see that the integration over t-channel variable for the above contributions is straightforward. This is not the case for the box diagrams since the box loop integrals depend explicitly on the t and u channel variables.

### III. CONTRIBUTION FROM THE BOX DIAGRAMS

The total box contribution to the process  $q\bar{q} \rightarrow t\bar{t}$  can be written as

$$M_{\text{box}}M_0^\dagger = M_{\text{box}}^{\text{DB}}M_0^\dagger + M_{\text{box}}^{\text{CB}}M_0^\dagger \quad (38)$$

where

$$M_{\text{box}}^{\text{DB}}M_0^\dagger = \frac{7g_s^4}{432\hat{s}} \sum_i F_i^{\text{DB}} \quad (39)$$

Here  $i=0,11,12,13,23,24,25,26$  and 27. By using the notation

$$A_5^+ A_5^+ = [a_1^2 + b_1^2][\tilde{a}_1^2 + \tilde{b}_1^2] + 4a_1 b_1 \tilde{a}_1 \tilde{b}_1 \quad (40)$$

$$A_{5x} A_{5x} = [a_1^2 + b_1^2][\tilde{a}_1^2 + \tilde{b}_1^2] - 4a_1 b_1 \tilde{a}_1 \tilde{b}_1 \quad (41)$$

$$A_5^+ A_{5x} = [a_1^2 - b_1^2][\tilde{a}_1^2 + \tilde{b}_1^2] \quad (42)$$

we find for the direct-box diagram [Fig. 4a] contribution:

$$F_0^{DB} = \frac{\alpha_s}{\pi} [m_{\tilde{g}}^2 (2A_{5x} A_{5x}) [2\hat{s}m_t^2 + 2(\hat{t} - m_t^2)^2]] D_0 \quad (43)$$

$$F_{11}^{DB} = \frac{\alpha_s}{\pi} [m_{\tilde{g}} m_t (2A_5^+ A_{5x}) [-2\hat{s}^2]] D_{11} \quad (44)$$

$$F_{12}^{DB} = \frac{\alpha_s}{\pi} [m_{\tilde{g}} m_t (2A_5^+ A_{5x}) [2\hat{s}(\hat{s} - 2m_t^2) - 4(\hat{t} - m_t^2)^2]] D_{12} \quad (45)$$

$$F_{13}^{DB} = \frac{\alpha_s}{\pi} [-m_{\tilde{g}} m_t (2A_5^+ A_{5x}) [2\hat{s}(\hat{s} - 2m_t^2) - 4(\hat{t} - m_t^2)^2]] D_{13} \quad (46)$$

$$F_{22}^{DB} = \frac{\alpha_s}{\pi} [m_t^2 (2A_5^+ A_5^+) [2\hat{s}m_t^2 + 2(\hat{t} - m_t^2)^2 - 2\hat{s}^2]] D_{22} \quad (47)$$

$$F_{23}^{DB} = \frac{\alpha_s}{\pi} [m_t^2 (2A_5^+ A_5^+) [2\hat{s}m_t^2 + 2(\hat{t} - m_t^2)^2 - 2\hat{s}^2]] D_{23} \quad (48)$$

$$F_{24}^{DB} = \frac{\alpha_s}{\pi} [m_t^2 (2A_5^+ A_5^+) [2\hat{s}^2]] D_{24} \quad (49)$$

$$F_{25}^{DB} = \frac{\alpha_s}{\pi} [(2A_5^+ A_5^+) [2\hat{s}(\hat{u} - m_t^2)^2]] D_{25} \quad (50)$$

$$F_{26}^{DB} = \frac{\alpha_s}{\pi} [(2A_5^+ A_5^+) [2\hat{s}^2 m_t^2 - 2m_t^2 (2\hat{s}m_t^2 + 2(\hat{t} - m_t^2)^2) - 2\hat{s}(\hat{u} - m_t^2)^2]] D_{26} \quad (51)$$

$$F_{27}^{DB} = \frac{\alpha_s}{\pi} [-2(2A_5^+ A_5^+) [2\hat{s}m_t^2 + 2(\hat{u} - m_t^2)^2]] D_{27} \quad (52)$$

In the above, the arguments of the D-functions are  $D_i = D_i[-p_1, p_3, p_4, m_{\tilde{q}_1}, m_{\tilde{g}}, m_{\tilde{t}_1}, m_{\tilde{g}}]$ .

For the contribution of the crossed-box diagram [Fig. 4b], we find

$$M_{\text{box}}^{\text{CB}} M_0^\dagger = [-\frac{2}{7}] \frac{7g_s^4}{432 \hat{s}} \sum_i F_i^{\text{CB}} \quad (53)$$

with

$$\overline{A_5^+ A_{5x}} = -[a_1^2 + b_1^2][\tilde{a}_1^2 - \tilde{b}_1^2] \quad (54)$$

$$F_0^{CB} = \frac{\alpha_s}{\pi} [m_{\tilde{g}}^2 (2A_{5x} A_{5x}) [2\hat{s}m_t^2 + 2(\hat{u} - m_t^2)^2]] D_0 \quad (55)$$

$$F_{11}^{CB} = \frac{\alpha_s}{\pi} [m_{\tilde{g}} m_t (\overline{2A_5^+ A_{5x}}) [-2\hat{s}^2]] D_{11} \quad (56)$$

$$F_{12}^{CB} = \frac{\alpha_s}{\pi} [m_{\tilde{g}} m_t (\overline{2A_5^+ A_{5x}}) [2\hat{s}(\hat{s} - 2m_t^2) - 4(\hat{u} - m_t^2)^2]] D_{12} \quad (57)$$

$$F_{13}^{CB} = \frac{\alpha_s}{\pi} [-m_{\tilde{g}} m_t (\overline{2A_5^+ A_{5x}}) [2\hat{s}(\hat{s} - 2m_t^2) - 4(\hat{u} - m_t^2)^2]] D_{13} \quad (58)$$

$$F_{22}^{CB} = \frac{\alpha_s}{\pi} [m_t^2 (2A_5^+ A_5^+) [2\hat{s}m_t^2 + 2(\hat{u} - m_t^2)^2 - 2\hat{s}^2]] D_{22} \quad (59)$$

$$F_{23}^{CB} = \frac{\alpha_s}{\pi} [m_t^2 (2A_5^+ A_5^+) [2\hat{s}m_t^2 + 2(\hat{u} - m_t^2)^2 - 2\hat{s}^2]] D_{23} \quad (60)$$

$$F_{24}^{CB} = \frac{\alpha_s}{\pi} [m_t^2 (2A_5^+ A_5^+) [2\hat{s}^2]] D_{24} \quad (61)$$

$$F_{25}^{CB} = \frac{\alpha_s}{\pi} [(2A_5^+ A_5^+) [2\hat{s}(\hat{t} - m_t^2)^2]] D_{25} \quad (62)$$

$$F_{26}^{CB} = \frac{\alpha_s}{\pi} [(2A_5^+ A_5^+) [2\hat{s}^2 m_t^2 - 2m_t^2 (2\hat{s}m_t^2 + 2(\hat{u} - m_t^2)^2) - 2\hat{s}(\hat{t} - m_t^2)^2]] D_{26} \quad (63)$$

$$F_{27}^{CB} = \frac{\alpha_s}{\pi} [-2(2A_5^+ A_5^+) [2\hat{s}m_t^2 + 2(\hat{t} - m_t^2)^2]] D_{27} \quad (64)$$

In the above, the arguments of the D-functions are  $D_i = D_i[-p_1, p_4, p_3, m_{\tilde{q}_1}, m_{\tilde{g}}, m_{\tilde{t}_1}, m_{\tilde{g}}]$ .

We are now in a position to write the expression for top pair production in proton anti-proton collision by weighing our expressions for differential cross section and cross section of the subprocess  $q\bar{q} \rightarrow t\bar{t}$  by the parton distribution functions and integrating over the parton variables i.e.,

$$d\sigma(p\bar{p} \rightarrow t\bar{t}) = \sum_{i,j} \int_0^1 dx_1 \int_0^1 dx_2 [D_{i/p}(x_1, Q^2) D_{j/\bar{p}}(x_2, Q^2)] d\hat{\sigma}(ij \rightarrow t\bar{t}) \quad (65)$$

Here  $d\hat{\sigma}$  represents the subprocess cross section at c.m. energy square of  $\hat{s} = x_1 x_2 s$ , where  $\sqrt{s}$  is the c.m. energy of the  $p\bar{p}$  system. In our numerical calculation, we adopt the MRSA parametrization [14] for effective parton distribution evaluated at  $Q^2 = m_t^2$ . In order to show the SUSY radiative corrections clearly, we use a constant  $\alpha_s = 0.123$ .

#### IV. NUMERICAL RESULTS AND CONCLUSIONS

To facilitate comparison with work of [8] we give our numerical results for the same parameter values as in [8]. A more detailed numerical work will be given elsewhere. We thus take  $m_t = 170$  GeV, and assume no mixing between the squarks. The mass splitting between the squarks of different flavors is also ignored [8]. The common squark mass is denoted by  $m_{\tilde{q}}$ .

We first consider percentage one loop corrections at the hadronic cross section as a function of the squark mass. Taking the gluino mass to be 150 GeV we find the percentage corrections changes from  $-5.3\%$  [ $m_{\tilde{q}} = 100$  GeV] to  $1\%$  [ $m_{\tilde{q}} = 600$  GeV], see the solid curve of Fig. 5. This does not agree with the original claim of Li *et al.* [8], where they find for gluino mass of 150 GeV,  $23\%$  [ $m_{\tilde{q}} = 100$  GeV] and  $5\%$  [ $m_{\tilde{q}} = 420$  GeV]. However, the

corrected version [8][see Erratum] values of  $-6\%$  [ $m_{\tilde{q}} = 100$  GeV] and  $4\%$  [ $m_{\tilde{q}} = 600$  GeV] for gluino mass of 150 GeV are in more closer agreement with our values. The remaining small discrepancy may probably be explained since they [8] have not included the gluon self-energy and the crossed box. For gluino mass of 200 GeV we find, see Fig. 5b, that the corrections change rapidly from 22% to  $-0.5\%$  as squark mass changes from 100 GeV to 600 GeV. Here again there is no agreement with the original claim of [8] where they had reported a variation of 6.5% to 0% for a gluino mass of 200 GeV. The revised [erratum [8]] values of 31% [squark mass of 100 GeV] and 6% [squark mass 600 GeV] for gluino mass of 200 GeV, are still somewhat different from our values. We find for the gluino mass of 200 GeV, the relative corrections of 22%, 9%, 6%, 3%, 1%,  $-0.5\%$  for  $m_{\tilde{q}} = 100, 200, 300, 400, 500, 600$  GeV respectively, which should be compared with 31%, 18%, 11%, 9%, 7%, 6% of the revised values of [8].

A comment is in order. It can be noticed from our Fig. 5 that the corrections change sign as the gluino mass is changed from 150 GeV to 200 GeV. As we have assumed a top mass of 170 GeV the threshold for top pair production is crossed in this region and hence the sign change and rapid change in magnitude of relative corrections occur.

Next let us consider percentage one loop corrections at the hadronic differential cross section as a function of the squark mass. As an example, we show the case at the  $t\bar{t}$  center-of-mass scattering angle  $\theta_{cm} = 10^\circ$ . Taking the gluino mass to be 150 GeV we find the percentage corrections changes from  $-7.5\%$  [ $m_{\tilde{q}} = 100$  GeV] to  $2.5\%$  [ $m_{\tilde{q}} = 600$  GeV], see the solid curve in Fig. 6. For gluino mass of 200 GeV we find, see the dashed curve in Fig. 6, that the corrections change rapidly from 22% to 0% as squark mass changes from 100 GeV to 600 GeV. As remarked before it is only the box loop correction which depends on the t-channel variable or on  $\theta_{cm}$ . If the box corrections are not larger than the other contributions, one would naively expect the percentage differential cross section to show only a weak dependence

on  $\theta_{cm}$ . This is indeed the case as can be seen by comparing Figs. 5 and 6.

It is useful to give the percentage correction at the parton level since among other things they facilitate a comparison with correction found in the context of standard model [9]. Moreover the corrections at the parton level can provide more direct and detailed tests of SUSY corrections. We first show in Fig. 7 the percentage corrections to the  $q\bar{q} \rightarrow t\bar{t}$  cross section as functions of the subprocess c.m. energy  $\sqrt{\hat{s}}$ . At the parton level the total percentage cross section varies between 20% and -9% as center of mass energy is varied between 350 GeV to 1.8 TeV. When gluino mass is 150 GeV (the solid line), the correction is positive very near to the threshold ( $\sqrt{\hat{s}} < 430$  GeV) but it gets rapidly negative down to -9% at around  $\sqrt{\hat{s}} \approx 800$  GeV. The resulting cancellation explains the smallness of the correction at the hadronic level; see the solid line at  $m_{\tilde{q}} = 200$  GeV in Fig. 5. For  $m_{\tilde{g}} = 200$  GeV (the dashed line), the correction grows from about 7% near the threshold to 20% at  $\sqrt{\hat{s}} = 400$  GeV where the gluino-pair threshold opens. This large positive correction slightly above the  $t\bar{t}$  threshold explains the large positive correction to the hadronic cross section in Figs. 5 and 6. We may compare these results to the standard model [9] who report on the one loop virtual [electroweak] relative corrections to parton  $q\bar{q} \rightarrow t\bar{t}$  cross section among other things. As they take the top mass of 100 GeV and 250 GeV we can't compare our results directly with theirs. However we can extrapolate from their Figs. 9 and 10 that for a top-quark mass of 170 GeV one would obtain corrections between 350 GeV and 1.8 TeV of around 10% and -15%.

In order to clarify structure of the SUSY radiative corrections, we show in Figs. 8a and 8b contributions from the gluon self-energy correction (dotted line), the sum of the triangle and quark wave-function corrections (short-dash), the direct-box (long-dash) and the crossed-box (dash-dotted) contributions separately. Fig. 8a is for  $m_{\tilde{g}} = 150$  GeV and Fig. 8b is for  $m_{\tilde{g}} = 200$  GeV, while all the squark masses are set to 200 GeV in both

cases. While the gluon self-energy correction grows with energy, the sum of the triangle and quark wave-function corrections more than compensate for the effects. Direct box diagram contribution is positive near the threshold and turns to negative at higher energies. The crossed box diagram partially cancels the direct box contribution. Box contributions are generally smaller than the other corrections as expected from the similarity of the corrections to the total and differential cross sections. The gluino-pair threshold effects are evident in all the curves in Fig. 8b.

We finally consider the percentage corrections at the parton level taking  $\sqrt{\hat{s}} = 600$  GeV and letting the squark mass vary between 100 GeV and 600 GeV. For the gluino mass of 150 GeV we find that the percentage corrections of differential cross section vary between  $-20\%$  and  $6.5\%$ , [Fig. 9]. For the gluino mass of 200 GeV the corrections vary between  $-7\%$  and  $4\%$ , [Fig. 9].

**Note added:** After the calculation was completed and the present paper was being written up: the following works came to our attention:

1: J. Kim *et al.* [17] examine both the SUSY Electroweak and SUSY QCD like correction. However they do not include box diagrams and claim that the box contributions are small citing J. Ellis and D. Ross, [11] and P. Kraus and F. Wilczek, [18] works as evidence. These authors state that their results for SUSY QCD agree with Ref. [8] while those of SUSY Electroweak disagree with J. Yang and C.S. Li [10].

2: J. Ellis and D. Ross [11] work at the parton level considering the processes  $q\bar{q} \rightarrow q\bar{q}$ ,  $q\bar{q} \rightarrow qq$ ,  $q\bar{q} \rightarrow gg$ , and  $qg \rightarrow qg$ . However they do not consider  $t\bar{t}$  cross section as it requires separate treatment.

3: P. Krauss and F. Wilczek [18] also studied the SUSY corrections to the quark gluon scattering processes in the limit of large SUSY particle masses.



## ACKNOWLEDGEMENTS

The authors would like to thank S.Y. Choi, C.S Kim, and R. Szapalski for useful suggestions and helpful comments. We would like to thank R. Rangarajan for bringing Li *et al.* [8] to our attention. The work of SA is supported by COE fellowship of the Japanese Ministry of Education, Science and Culture [MONBUSHO], that of KH by the Grant-in-Aid for Scientific Research from the Japanese Ministry of Education, Science and Culture (No. 05228104), and that of SM is supported by Japan Society for the Promotion of Science (No. 2474).

## REFERENCES

- [1] CDF Collaboration, F. Abe *et al.*, Phys. Rev. Lett. **74**, 2676 (1995).
- [2] D0 Collaboration, S. Abachi *et al.*, Phys. Rev. Lett. **74**, 2632 (1995).
- [3] E. Berger and H. Contopoulos, Phys. Lett. **B361**, 115 (1995) and hep-ph/9603326.
- [4] K. Hagiwara, Talk presented at XVII Int. Symp. on Lepton and Photon Interactions at High Energies, 10-15 August 1995, Beijing, to appear in the proceedings, hep-ph/9512425.
- [5] Particle Data Group, L Montanet et al., Phys. Rev. **D50**, 1173 (1995).
- [6] S. Eidelman and F. Jegerlehner, Z. Phys. **C67**, 602 (1995).
- [7] D. Amidei and R. Brock eds., FERMILAB-PUB-96/082.
- [8] C.S. Li, B.Q. Hu, J.M. Yang, and C.G. Hu Phys. Rev. **D52**, 5014 (1995), *ibid* [Erratum]**D53**, 4112 (1996).
- [9] W. Beenakker, A. Denner, W. Hollik, R. Mertig, T. Sack and D. Wackeroth, Nucl. Phys. **B411**, 343 (1994).
- [10] A. Stange and S. Willenbrock Phys. Rev. **D48**, 2054 (1993), see also J.M. Yang and C.S. Li, Phys. Rev. **D52**, 1541 (1995). There is an erratum to the latter paper as pointed out in ref. [17]
- [11] J. Ellis and D. Ross, hep-ph/9604432.
- [12] G.J. van Oldenborgh and J.A.M. Vermaseren, Z. Phys. **C46**, 425 (1990).
- [13] G. Passarino and M. Veltman, Nucl. Phys. **B160**, 151 (1979).

- [14] A.D. Martin, R. Roberts, W.J. Stirling, Phys. Rev. **D50**, 6734 (1994).
- [15] S. Kawabata, Computer Physics Communications **88**,309 (1995).
- [16] H.E. Haber and G.L. Kane, Phys. Rep. **117** , 75 (1985).
- [17] J. Kim, J.L Lopez, D.V. Nanopoulos and R. Rangarajan, hep-ph/9605419.
- [18] P. Kraus, and F. Wilczek, hep-ph/9601279.

## FIGURES

**Fig. 1** Tree-Level Diagram for the process  $q\bar{q} \longrightarrow t\bar{t}$ .

**Fig. 2a** Schematic diagram for the Gluon Self-Energy due to SQCD particles.

**Fig. 2b** Schematic diagram for the Quark WFNR due to the SQCD particles.

**Fig. 2c** Schematic diagram for the Anti-Quark WFNR due to the SQCD particles.

**Fig. 2d** Schematic diagram for the Top WFNR due to the SQCD particles.

**Fig. 2e** Schematic diagram for the Anti-Top WFNR due to the SQCD particles.

**Fig. 3a** Triangle contribution from two stops and one gluino to the  $t\bar{t}g$  vertex.

**Fig. 3b** Triangle contribution from two squarks and one gluino to the  $q\bar{q}g$  vertex.

**Fig. 3c** Triangle contribution from one stop and two gluinos to the  $t\bar{t}g$  vertex.

**Fig. 3d** Triangle contribution from one squark and two gluinos to the  $q\bar{q}g$  vertex.

**Fig. 4a** Direct Box contribution from one stop, one squark and two gluinos.

**Fig. 4b** Crossed Box contribution from one stop, one squark and two gluinos.

**Fig. 5** One-loop percentage relative corrections to the  $t\bar{t}$  production cross section in  $p\bar{p}$  collisions at  $\sqrt{s} = 1.8$  TeV as a function of squark mass for a gluino mass of 150 GeV (solid line) and 200 GeV (dashed line). The top quark mass is set to 170 GeV.

**Fig. 6** One-loop percentage relative corrections to the  $t\bar{t}$  production differential cross section at  $\theta_{\text{cm}} = 10^\circ$  in  $p\bar{p}$  collisions at  $\sqrt{s} = 1.8$  TeV. The results are shown for  $m_t = 170$  GeV as functions of the squark mass for a gluino mass of 150 GeV (solid line) and 200 GeV (dashed line).

**Fig. 7** One-loop percentage relative correction to the parton-level  $q\bar{q} \rightarrow t\bar{t}$  cross section for  $m_t = 170$  GeV as functions of the  $q\bar{q}$  center of mass energy,  $\sqrt{\hat{s}}$ . The results are shown for  $m_{\tilde{q}} = 200$  GeV and  $m_{\tilde{g}} = 150$  GeV (solid line) or  $m_{\tilde{g}} = 200$  GeV (dashed line).

**Fig. 8a** Individual contributions of the one-loop percentage relative correction to the  $q\bar{q} \rightarrow t\bar{t}$  cross section are given as functions of the  $q\bar{q}$  c.m. energy  $\sqrt{\hat{s}}$ . Gluon self-energy correction (dotted line), the sum of triangle and quark wave-function corrections (short-dashed line), the direct-box diagram (long-dashed line) and the crossed-box diagram contributions (dash-dotted line) are shown separately. Also shown by the solid line is the total percentage relative correction, as given in Fig. 7. The mass parameters are:  $m_t = 170$  GeV,  $m_{\tilde{q}} = 200$  GeV, and  $m_{\tilde{g}} = 150$  GeV.

**Fig. 8b** Same as Fig. 8a except  $m_{\tilde{g}} = 200$  GeV.

**Fig. 9** One-loop percentage relative corrections to the parton-level  $q\bar{q} \rightarrow t\bar{t}$  differential cross section at  $\theta_{\text{cm}} = 10^\circ$  and  $\sqrt{\hat{s}} = 600$  GeV. The results are shown for  $m_t = 170$  GeV as functions of the squark mass for a gluino mass of 150 GeV (solid line) and 200 GeV (dashed line).

## APPENDIX: CONTRIBUTION FROM THE BOX DIAGRAMS

As already mentioned we give in this appendix the box results in the notation of Li *et al.* [8], for the purposes of exact comparison. The total box contribution to the process  $q\bar{q} \longrightarrow t\bar{t}$  can be written as

$$M_{\text{box}} M_0^\dagger = M_{\text{box}}^{\text{DB}} M_0^\dagger + M_{\text{box}}^{\text{CB}} M_0^\dagger \quad (\text{A1})$$

where

$$M_{\text{box}}^{\text{DB}} M_0^\dagger = \frac{7g_s^4}{432\hat{s}} \sum_i F_i^{\text{DB}} \quad (\text{A2})$$

Here  $i=0,11,12,13,23,24,25,26$  and 27.

$$A_5^+ A_5^+ = [a_1^2 + b_1^2][\tilde{a}_1^2 + \tilde{b}_1^2] + 4a_1 b_1 \tilde{a}_1 \tilde{b}_1 \quad (\text{A3})$$

$$A_{5x} A_{5x} = [a_1^2 + b_1^2][\tilde{a}_1^2 + \tilde{b}_1^2] - 4a_1 b_1 \tilde{a}_1 \tilde{b}_1 \quad (\text{A4})$$

$$A_5^+ A_{5x} = [a_1^2 - b_1^2][\tilde{a}_1^2 + \tilde{b}_1^2] \quad (\text{A5})$$

We note that the following relations hold between our A's and  $\sigma$ 's of [8]

$$\begin{aligned} 2A_5^+ A_5^+ &= \sigma_{ij}^2 + \lambda_{ij}^2 \\ 2A_5^+ A_{5x} &= \sigma_{ij} \sigma'_{ij} + \lambda_{ij} \lambda'_{ij} \\ 2A_{5x} A_{5x} &= \sigma_{ij}'^2 + \lambda_{ij}'^2 \end{aligned} \quad (\text{A6})$$

$$F_0^{DB} = \frac{\alpha_s}{\pi} [m_{\tilde{g}}^2 (2A_{5x} A_{5x}) [2\hat{s} m_t^2 + 2(\hat{t} - m_t^2)^2] + m_{\tilde{g}} m_t (2A_5^+ A_{5x}) [2\hat{s}^2]] D_0 \quad (\text{A7})$$

$$F_{11}^{DB} = \frac{\alpha_s}{\pi} [m_{\tilde{g}} m_t (2A_5^+ A_{5x}) [2\hat{s}^2]] D_{11} \quad (\text{A8})$$

$$F_{12}^{DB} = \frac{\alpha_s}{\pi} [-m_t^2 (2A_5^+ A_5^+) [2\hat{s}m_t^2 + 2(\hat{u} - m_t^2)^2] - m_{\tilde{g}}m_t (2A_5^+ A_{5x}) [2\hat{s}^2]] D_{12} \quad (A9)$$

$$F_{13}^{DB} = \frac{\alpha_s}{\pi} [m_t^2 (2A_5^+ A_5^+) [2(\hat{u} - m_t^2)^2] - m_{\tilde{g}}m_t (2A_5^+ A_{5x}) [2\hat{s}(\hat{s} - 2m_t^2) - 4(\hat{t} - m_t^2)^2]] D_{13} \quad (A10)$$

$$F_{23}^{DB} = \frac{\alpha_s}{\pi} [m_t^2 (2A_5^+ A_5^+) [2\hat{s}m_t^2 + 2(\hat{t} - m_t^2)^2 - 2\hat{s}^2]] D_{23} \quad (A11)$$

$$F_{24}^{DB} = \frac{\alpha_s}{\pi} [-(2A_5^+ A_5^+) [2\hat{s}^2m_t^2 + 2\hat{s}(\hat{u} - m_t^2)^2]] D_{24} \quad (A12)$$

$$F_{25}^{DB} = \frac{\alpha_s}{\pi} [(2A_5^+ A_5^+) [2\hat{s}(\hat{u} - m_t^2)^2]] D_{25} \quad (A13)$$

$$F_{26}^{DB} = \frac{\alpha_s}{\pi} [m_t^2 (2A_5^+ A_5^+) [2\hat{s}^2]] D_{26} \quad (A14)$$

$$F_{27}^{DB} = \frac{\alpha_s}{\pi} [-2(2A_5^+ A_5^+) [2\hat{s}m_t^2 + 2(\hat{u} - m_t^2)^2]] D_{27} \quad (A15)$$

Here the arguments of the D-functions are  $D_i = D_i[-p_1, -p_2, p_4, m_{\tilde{g}}, m_{\tilde{q}_i}, m_{\tilde{g}}, m_{\tilde{t}_i}]$ . The above results for the direct box agree with [8] after taking account of their erratum.

Although Ref. [8] does not give the contributions of the crossed-box diagram, we give our result in their notation.

$$M_{\text{box}}^{\text{CB}} M_0^\dagger = [-\frac{2}{7}] \frac{7g_s^4}{432 \hat{s}} \sum_i F_i^{\text{CB}} \quad (A16)$$

Here  $i=0,11,12,13,23,24,25,26$  and 27. We note that the crossed box color factor is smaller by a factor of  $\frac{2}{7}$  compared to the direct box, and it contributes destructively with the direct-box contribution; see Eq. A1.

$$\overline{A_5^+ A_{5x}} = -[a_1^2 + b_1^2][\tilde{a}_1^2 - \tilde{b}_1^2] \quad (A17)$$

$$F_0^{CB} = \frac{\alpha_s}{\pi} [m_{\tilde{g}}^2 (2A_{5x} A_{5x}) [2\hat{s}m_t^2 + 2(\hat{u} - m_t^2)^2] + m_{\tilde{g}} m_t (\overline{2A_5^+ A_{5x}}) [2\hat{s}^2]] D_0 \quad (\text{A18})$$

$$F_{11}^{CB} = \frac{\alpha_s}{\pi} [m_{\tilde{g}} m_t (\overline{2A_5^+ A_{5x}}) [2\hat{s}^2]] D_{11} \quad (\text{A19})$$

$$F_{12}^{CB} = \frac{\alpha_s}{\pi} [-m_t^2 (2A_5^+ A_5^+) [2\hat{s}m_t^2 + 2(\hat{t} - m_t^2)^2] - m_{\tilde{g}} m_t (\overline{2A_5^+ A_{5x}}) [2\hat{s}^2]] D_{12} \quad (\text{A20})$$

$$F_{13}^{CB} = \frac{\alpha_s}{\pi} [m_t^2 (2A_5^+ A_5^+) [2(\hat{t} - m_t^2)^2] - m_{\tilde{g}} m_t (\overline{2A_5^+ A_{5x}}) [2\hat{s}(\hat{s} - 2m_t^2) - 4(\hat{u} - m_t^2)^2]] D_{13} \quad (\text{A21})$$

$$F_{23}^{CB} = \frac{\alpha_s}{\pi} [m_t^2 (2A_5^+ A_5^+) [2\hat{s}m_t^2 + 2(\hat{u} - m_t^2)^2 - 2\hat{s}^2]] D_{23} \quad (\text{A22})$$

$$F_{24}^{CB} = \frac{\alpha_s}{\pi} [-(2A_5^+ A_5^+) [2\hat{s}^2 m_t^2 + 2\hat{s}(\hat{t} - m_t^2)^2]] D_{24} \quad (\text{A23})$$

$$F_{25}^{CB} = \frac{\alpha_s}{\pi} [(2A_5^+ A_5^+) [2\hat{s}(\hat{t} - m_t^2)^2]] D_{25} \quad (\text{A24})$$

$$F_{26}^{CB} = \frac{\alpha_s}{\pi} [m_t^2 (2A_5^+ A_5^+) [2\hat{s}^2]] D_{26} \quad (\text{A25})$$

$$F_{27}^{CB} = \frac{\alpha_s}{\pi} [-2(2A_5^+ A_5^+) [2\hat{s}m_t^2 + 2(\hat{t} - m_t^2)^2]] D_{27} \quad (\text{A26})$$

Here the arguments of the D-functions are  $D_i = D_i[-p_1, -p_2, p_3, m_{\tilde{g}}, m_{\tilde{q}_i}, m_{\tilde{g}}, m_{\tilde{t}_i}]$ .

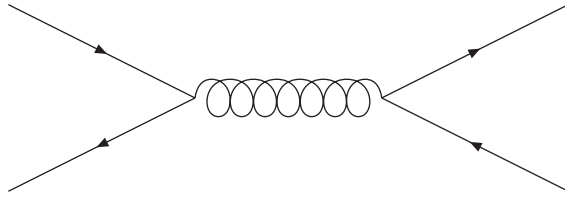


Fig.1: Tree-level Diagram

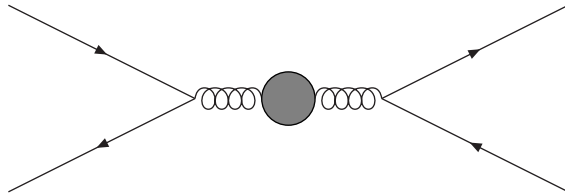


Fig.2a: Gluon Self Energy due to Particles

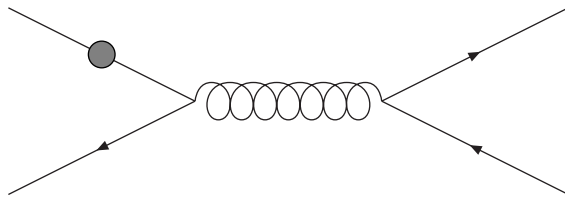


Fig.2b: Quark Self Energy due to SQCD Particles



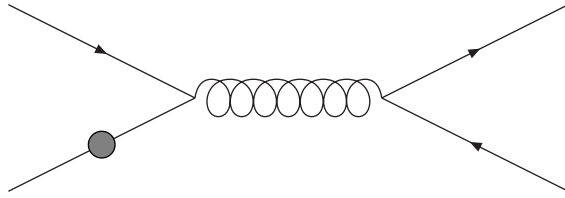


Fig.2c Anti-Quark Self Energy due to SQCD Particles

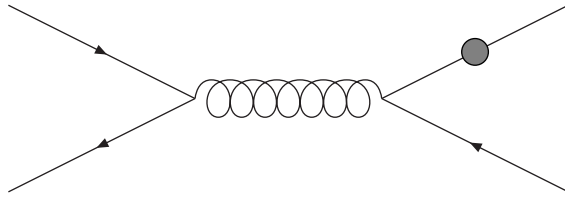


Fig.2d Top Self Energy due to SQCD Particles

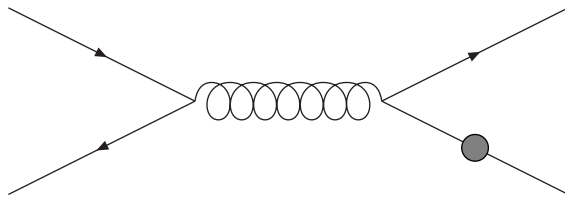


Fig.2e Anti-Top Self Energy due to SQCD Particles

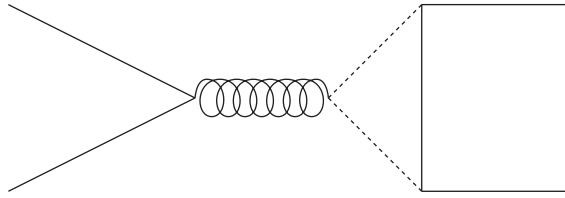


Fig.3a: Triangle contribution from two stops and one gluino

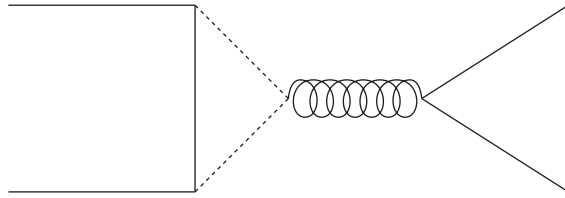


Fig.3b: Triangle contribution from two squarks and one gluino

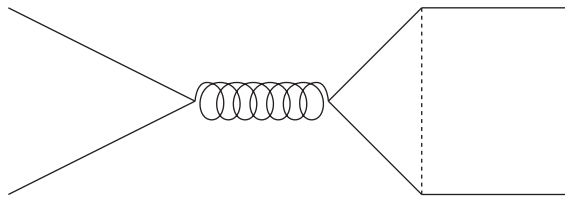


Fig.3c: Triangle contribution from two gluinos and one stops

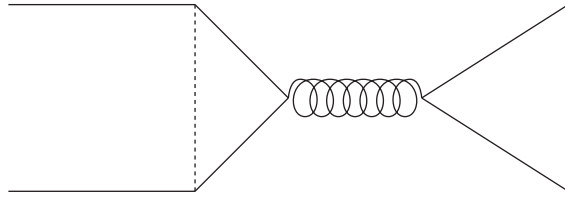


Fig.3d: Triangle contribution from two gluinos and one squark

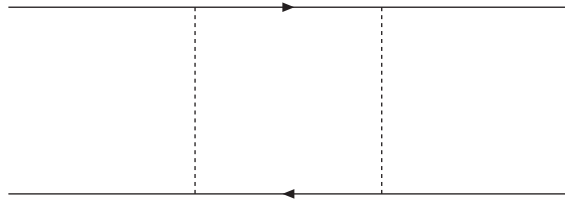


Fig.4a: Direct Box contribution from SQCD Particles

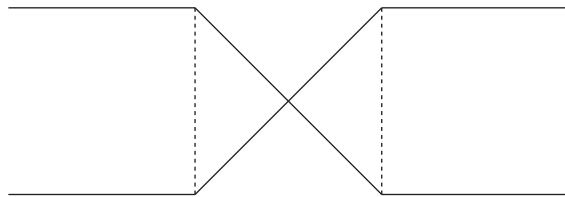


Fig.4b: Crossed Box contribution from SQCD Particles

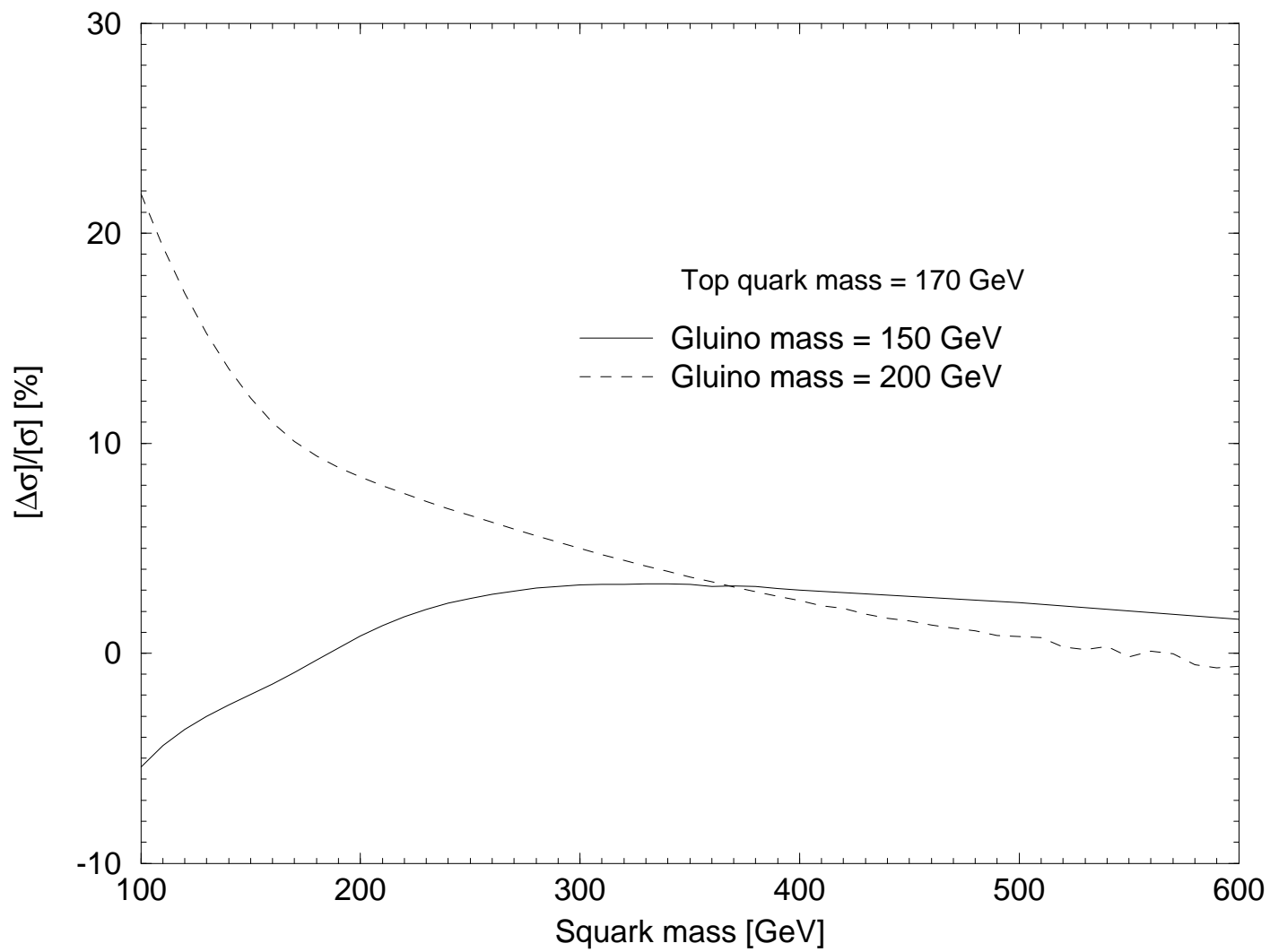


Fig. 5

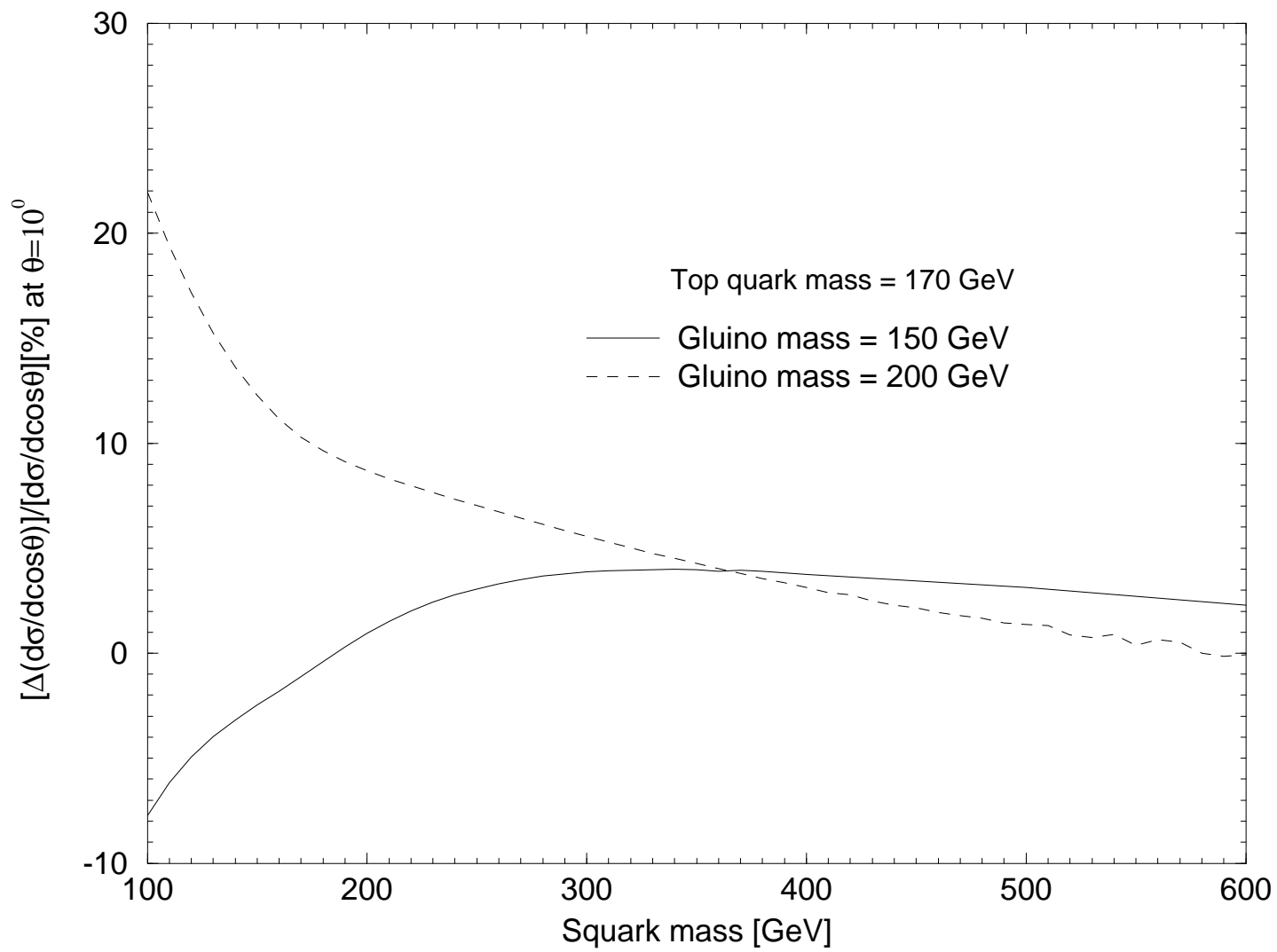


Fig. 6

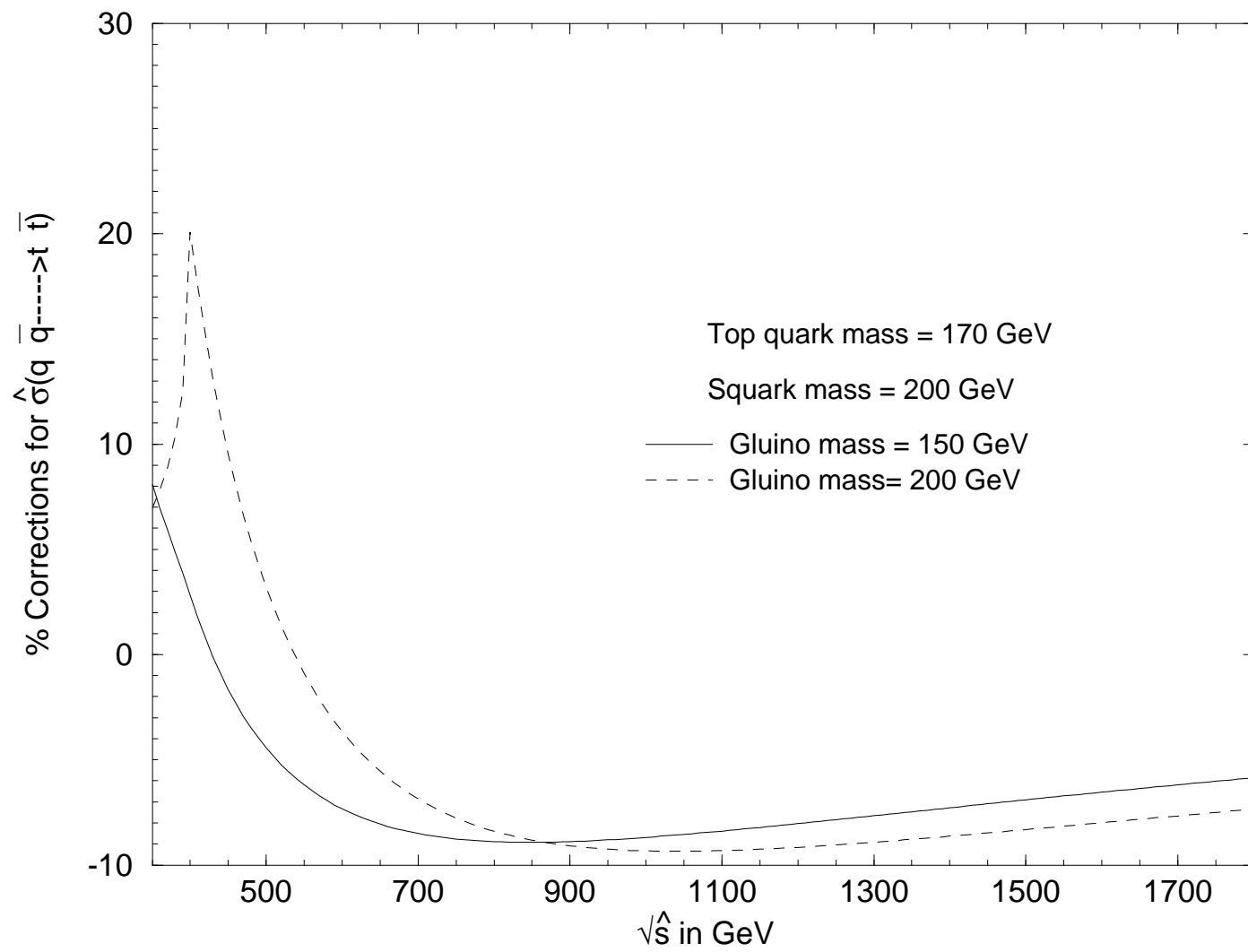


Fig. 7

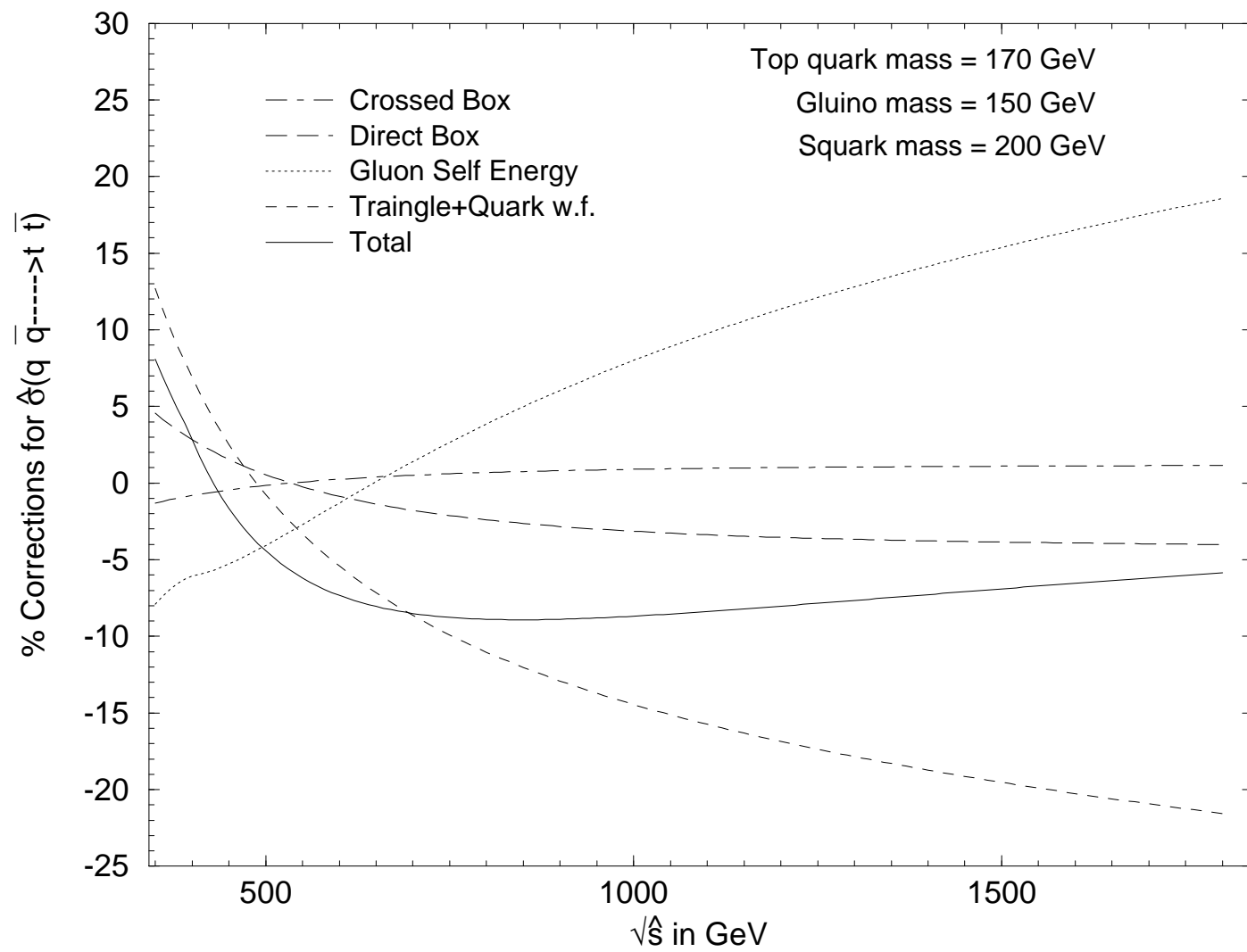


Fig. 8a

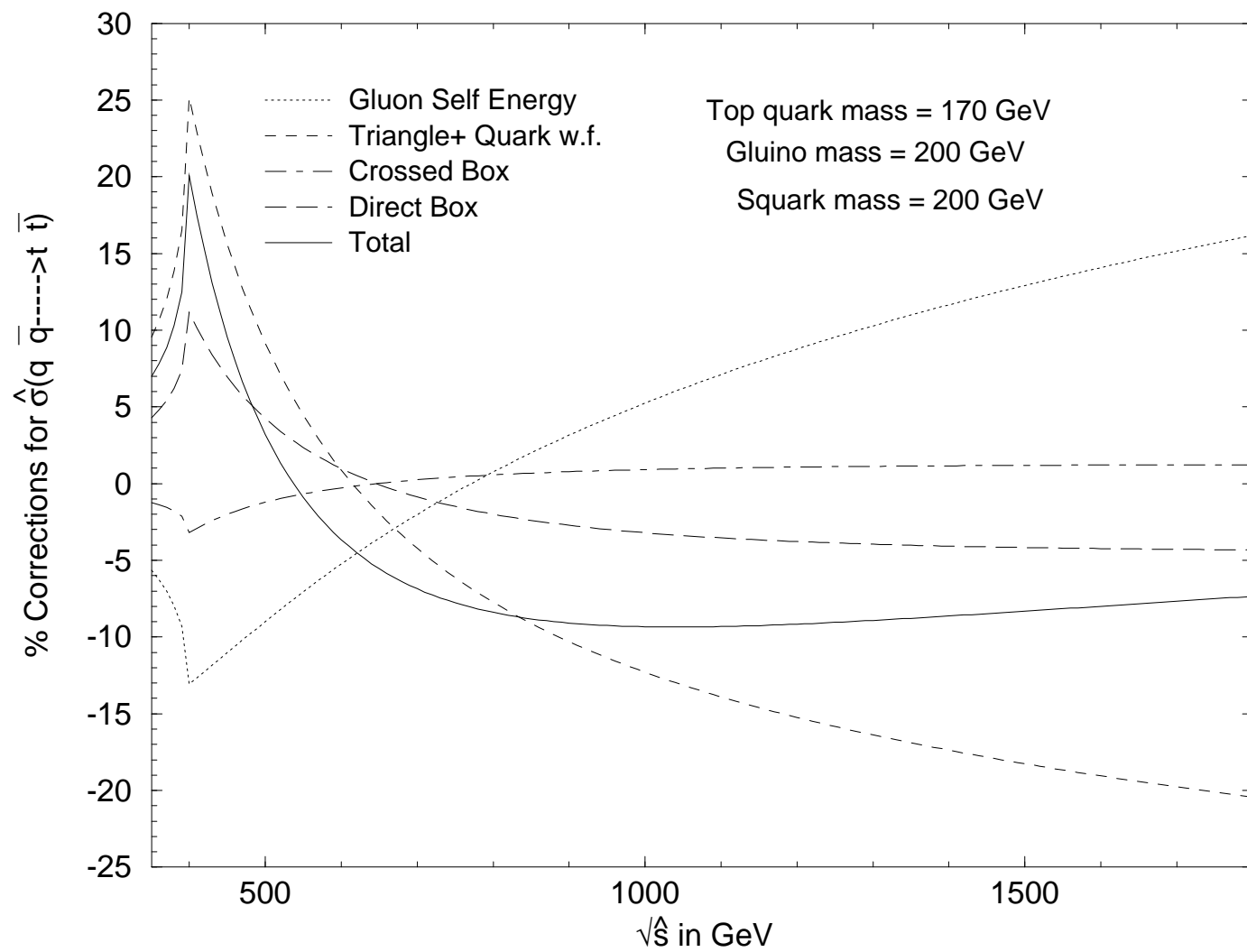


Fig. 8b



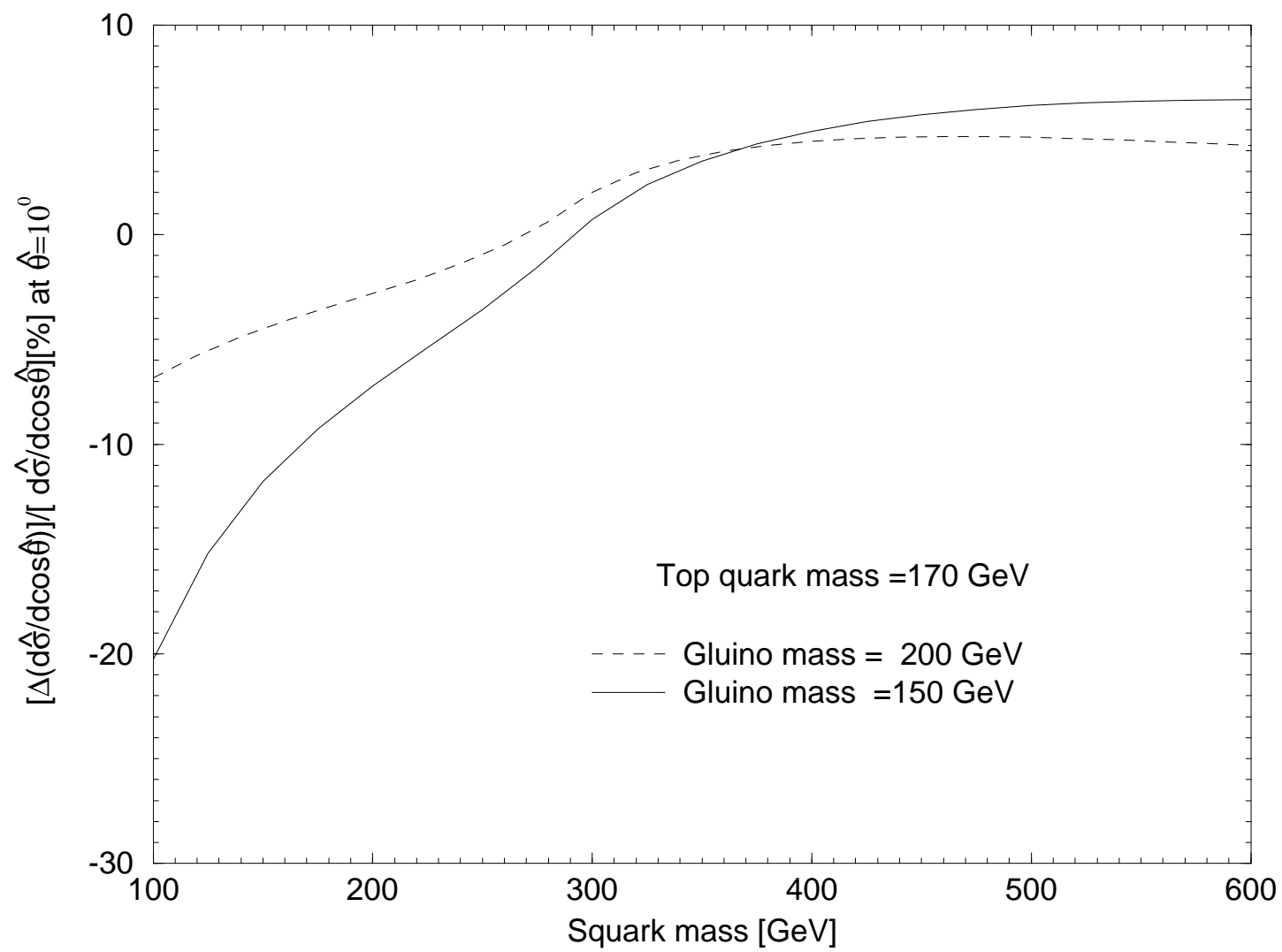


Fig. 9